arXiv:cond-mat/0111536v1 [cond-mat.str-el] 28 Nov 2001

Exchange coupling in $CaMnO_3$ and $LaMnO_3$: configuration interaction and the coupling mechanism

M. Nicastro and C.H. Patterson
Department of Physics and Centre for Scientific Computation, University of Dublin, Trinity College, Dublin 2, Ireland.
(February 1, 2008)

Abstract

The equilibrium structure and exchange constants of $CaMnO_3$ and $LaMnO_3$ have been investigated using total energy unrestricted Hartree-Fock (UHF) and localised orbital configuration interaction (CI) calculations on the bulk compounds and $Mn_2O_{11}^{14-}$ and $Mn_2O_{11}^{16-}$ clusters. The predicted structure and exchange constants for $CaMnO_3$ are in reasonable agreement with estimates based on its Néel temperature. A series of calculations on $LaMnO_3$ in the cubic perovskite structure shows that a Hamiltonian with independent orbital ordering and exchange terms accounts for the total energies of cubic $LaMnO_3$ with various spin and orbital orderings. Computed exchange constants depend on orbital ordering. Exchange contributions to the total energy vary between -20 and 20 meV per Mn ion, differences in orbital ordering energy vary between 3 and 100 meV and a Jahn-Teller distortion results in an energy reduction of around 300 meV. The lattice constant of the lowest energy cubic perovskite structure (3.953 Å) is in good agreement with the lattice constant of the high temperature 'cubic' phase of $LaMnO_3$ (3.947 Å). The total energy of *Pnma* $LaMnO_3$ was minimised by varying lattice parameters and seven internal coordinates and a structure 194 meV per Mn ion below that of a structure determined by neutron diffraction was found. This optimised structure is nearly isoenergetic with a cubic perovskite structure with a 5 percent Jahn-Teller distortion. UHF calculations tend to underestimate exchange constants in $LaMnO_3$, but have the correct sign when compared with values obtained by neutron scattering; exchange constants obtained from CI calculations are in good agreement with neutron scattering data provided the Madelung potential of the cluster is appropriate. Cluster CI calculations reveal a strong dependence of exchange constants on Mn d e_g orbital populations in both compounds. CI wave functions are analysed in order to determine which exchange processes are important in exchange coupling in $CaMnO_3$ and $LaMnO_3$.

71.27.+a 75.10.-b 75.50.-y

Typeset using REVTEX

I. INTRODUCTION

$CaMnO_3$ and $LaMnO_3$ are endpoint compounds in the series $Ca_{1-x}La_xMnO_3$, which has been thoroughly studied experimentally and theoretically[1]. They have relatively simple atomic and magnetic structures, their magnetic excitations are well described by a spin wave Hamiltonian[2,3] and exchange constants, J, are well established by neutron scattering[2,3] and from the Néel temperature[4,5]. Exchange coupling in manganites has been extensively studied using model Hamiltonian[6–8] and *ab initio* calculations[9–15]. This paper presents results of bulk *ab initio* Unrestricted Hartree-Fock (UHF) and cluster Configuration Interaction (CI) calculations of exchange constants for both compounds.

Exchange constants obtained from CI calculations are in excellent agreement with experiment and the localised orbital CI wavefunctions are analysed to determine which quantum fluctuations are most important in exchange coupling. Model Hamiltonian calculations have attributed the exchange coupling energy to O^{2-} to $Mn^{3+/4+}$ superexchange[6], Mn d^{4+} d^{4+}/Mn d^{5+} d^{3+} t_{2g} superexchange[7], or both[8]. Results of calculations presented below show that both exchange mechanisms operate and that O superexchange is the more important of the two. This was also found to be the case in the model Hamiltonian calculations of Meskine *et al.*[8].

CI cluster calculations provide detailed information on exchange couplings between neighbouring Mn ions, however a bulk electronic structure technique is required to study orbital ordering in $LaMnO_3$. Total energies of $LaMnO_3$ with A and G-type anti-ferromagnetic (A-AF and G-AF) and ferromagnetic (FM) spin orderings have been computed in several isovolume structures in order to establish whether or not orbital ordering and spin ordering terms in the Hamiltonian for $LaMnO_3$ are independent. Obviously exchange constants will depend on orbital ordering, as the latter determines which empty orbitals are available to participate in exchange coupling. However, it is not known whether the e_g electron density in $LaMnO_3$ for a particular orbital ordering depends on spin ordering. It is shown below that a common orbital ordering energy for any of several orbital orderings can be identified and that this energy is independent of spin ordering, to a high degree. Spin and orbital ordering terms in the Hamiltonian are therefore independent, although orbital ordering determines the exchange constants.

At low temperatures, $CaMnO_3$ exists in a cubic perovskite structure (lattice constant 3.73 Å) with G-AF magnetic ordering[4] and a Néel temperature of 130 K. Using the Rushbrooke-Wood formula[5], this Néel temperature implies an exchange constant J = 6.6 meV. Note that throughout this work the spin Hamiltonian is of the form due to Domb and Sykes[16]

$$H = \sum_{<ij>} J_{ij} \frac{\hat{S}_i . \hat{S}_j}{S^2} \tag{1}$$

$\hat{S}_i$ is a spin operator, S is the magnitude of the total spin for an ion and J_{ij} is the exchange constant for a pair of ions. This form is adopted for the Hamiltonian as it is the same as that adopted in modelling spin wave dispersion in neutron scattering studies[2,3], except for a small Dzyaloshinsky-Moriya term.

At low temperatures the space group of $LaMnO_3$ is *Pnma*[4]. The ground state magnetic structure is A-AF and the unit cell contains four formula units consisting of rotated and distorted octahedra. There is one more d electron per Mn ion (*c.f.* $CaMnO_3$), which occupies an e_g orbital and induces a Jahn-Teller distortion in each MnO_6 octahedron, resulting in three distinct Mn-O bond lengths of 1.91, 1.97 and 2.18 Å[17]. The occupied e_g orbital is a linear combination of $d_{x^2-y^2}$ and $d_{3z^2-r^2}$ orbitals. The largest orbital component lies along the most elongated Mn-O bond. The *Pnma* structure is shown in Fig. 1. *a*, *b* and *c* axes referred to below are indicated on this diagram. The results of a number of neutron and x-ray scattering studies of the structure of $LaMnO_3$[18–23] over a range of temperatures are summarised in Ref.[17]. The *Pnma* structure can be viewed as containing planes of Mn^{3+} ions, each joined to its in-plane neighbours by pairs of short (1.91 Å) and long (2.18 Å) Mn-O bonds. Each Mn^{3+} ion in a particular plane is coupled to Mn^{3+} ions in planes immediately above and below by two Mn-O bonds (1.97 Å). The symmetry of the *Pnma* structure is such that there is one in-plane (nearest neighbour) exchange constant ($J_\parallel$) and one out-of-plane constant ($J_\perp$). Both $J_\parallel$ and $J_\perp$ have been determined from two independent neutron scattering studies to be -6.7 and 4.8 meV, respectively,[2,3]. Thus there is FM coupling within planes and AF coupling between planes.

II. EXCHANGE COUPLING MECHANISM

The first comprehensive attempt to explain atomic and magnetic structures in doped and undoped manganites was made by Goodenough[24] in 1955. He assumed three classes of exchange interaction between neighbouring Mn ions in undoped $CaMnO_3$ and $LaMnO_3$ lattices. A specific ordering of *empty* e_g orbitals and relative orientations of pairs of empty e_g orbitals correponding to Goodenough's classification are illustrated in Fig. 2. When empty e_g orbitals are available on a pair of neighbouring Mn ions and are oriented towards one another (Fig. 2b) then AF coupling of the Mn ion spins is energetically favoured. This is because electrons from the central O^{2-} ion of either spin are postulated to delocalise onto both Mn ions simultaneously, owing to the favourable exchange interaction (Hund's rule) between the delocalised electron and the Mn ion spin. However, if the Mn ion spins are FM aligned, only the electron from the central O^{2-} ion with the same spin orientation as the Mn ions can delocalise onto either Mn ion, resulting in a higher energy for that state. Thus the empty orbital arrangement shown in Fig. 2b results in an AF coupling of Mn spins. This is a type I exchange interaction according to Goodenough[24]. When one empty e_g orbital is suitably oriented for O^{2-} ion electron delocalisation (Fig. 2c), FM coupling of the Mn ion spins is favoured. This is a type II interaction. Finally, when no empty hybrids are available (Fig. 2d), no delocalisation occurs. This is a type III interaction. This model has been used to explain the relative energies of A-AF, G-AF and FM magnetic states of $CaMnO_3$ and $LaMnO_3$ with a cubic perovskite structure[14]. In that work it was found that the relative energies of these magnetic structures could be explained by counting the numbers of each type of interaction in each magnetic state and calculating the relative energy of each type of interaction. For both $CaMnO_3$ and $LaMnO_3$ it was found that the type I AF interaction was more energetically favourable than the type II interaction by 10 meV[14]. The simplified description of exchange interactions just given assumes that an empty e_g orbital is either

available or not. However, empty e_g orbitals in $LaMnO_3$ are not purely $d_{x^2-y^2}$ or $d_{3z^2-r^2}$ in character[6]. The mixed character of the empty e_g orbital permits some exchange coupling even when the empty e_g orbital is not optimally oriented.

This type of reasoning was used by Millis[6] in a calculation of exchange coupling energies in $CaMnO_3$ and $LaMnO_3$. In that work configurations allowed by the Pauli principle in which one or two electrons hop from the central O^{2-} ion to one or both neighbouring Mn ions are considered. Configurations which differ by a single electron hop have a single hopping matrix element, t. Diagonal elements of the Hamiltonian are parametrised using the energy required to excite one electron or a pair of electrons from an O^{2-} ion to a Mn ion. In $CaMnO_3$ the configuration which is assumed to lead to stabilisation of the AF state over the FM state is one in which a pair of electrons on the O^{2-} ion is excited onto separate Mn^{4+} ions. If this were indeed the origin of exchange coupling in $CaMnO_3$ then one would expect this configuration to appear in an *ab initio* ground state CI wave function, but this is not the case. However, the main idea of this model, that more low energy configurations are available to singlet states than high spin multiplicity states, is in accord with results presented here.

CI cluster calculations of exchange constants in La_2CuO_4[25,26] and $KNiF_3$[27], which used delocalised molecular orbitals have been reported quite recently. CI cluster calculations described below were carried out in a localised orbital basis. The localised orbital basis provides a means of identifying the exchange coupling mechanism in terms of fluctuations of electrons between localised orbitals. These calculations were performed on $Mn_2O_{11}^{14-}$ and $Mn_2O_{11}^{16-}$ clusters representing fragments of $CaMnO_3$ and $LaMnO_3$. Details of the calculations, including the method used to generate the localised orbitals, details of a spherical array of point charges surrounding the clusters, *etc.* are given in Appendix A. The wavefunctions for the clusters contain orbitals which are partitioned into a (doubly-occupied) core orbital space, an active space containing the 2p orbitals of the O^{2-} ion situated between the two Mn ions in the cluster as well as singly-occupied Mn d orbitals and an external space containing unoccupied Mn d orbitals. The core orbital space contains 'core' electrons as well as valence electrons not in the active orbital space. The ions in the clusters treated quantum mechanically consisted of two corner sharing MnO_6 octahedra. The localised orbitals in the active space for the $Mn_2O_{11}^{14-}$ and $Mn_2O_{11}^{16-}$ clusters are shown in Figs. 3 and 4, respectively. The main electronic configuration for the $Mn_2O_{11}^{14-}$ cluster representing $CaMnO_3$ is one in which each Mn ion with a formal 4+ charge contains three t_{2g} electrons and each oxygen ion exists in a closed shell O^{2-} configuration. The actual charge on the Mn ions is significantly reduced as there is a covalent component to the Mn-O bonds, as can clearly be seen in the contour plot of the localised orbital with mainly O 2pz character in the top panel of Fig. 3. The actual Mn ion charge in $CaMnO_3$ is +2.13, according to a Mulliken population analysis of the UHF wave functions obtained for $CaMnO_3$. The formal charge on Mn ions in $LaMnO_3$ is 3+, however a Mulliken population analysis of UHF wave functions for $LaMnO_3$ yields a charge of +2.24 The O ion charges in the two compounds are -1.33 ($CaMnO_3$) and -1.75 and -1.82 ($LaMnO_3$). Exchange constants were calculated by finding the energy difference between the spin singlet and spin septet(nonet) states of the $Mn_2O_{11}^{14-}$ and $Mn_2O_{11}^{16-}$ clusters.

Wave functions were constructed from the localised orbitals shown in Figs. 3 and 4 and doubly occupied core orbitals. A septet state for the $Mn_2O_{11}^{14-}$ cluster was constructed from

six singly-occupied t_{2g} orbitals and doubly occupied O 2p orbitals localised on the central O ion in the cluster. The form of this wave function is

$$\psi^{septet} = A\Big(\{core\}(\phi_{xy,l}\phi_{xz,l}\phi_{yz,l}\phi_{xy,r}\phi_{xz,r}\phi_{yz,r})(\alpha\alpha\alpha\alpha\alpha\alpha)\Big) \tag{2}$$

A is the anti-symmetrising operator and the subscripts l or r on t_{2g} orbitals in Eq. 2 indicate that they are centred on the left or right Mn ion, respectively. $\{core\}$ is a product of doubly occupied orbitals in the core orbital space which includes the 2p orbitals on the central O^{2-}. This is the restricted open shell Hartree-Fock (ROHF) wave function for the septet state, constructed using localised molecular orbitals. Self-consistent field (SCF) ROHF wave functions can be computed using a number of standard electronic structure packages such as the GAMESS package[28] used in this work.

The singlet state is constructed from the same set of singly-occupied orbitals with a spin-coupling of the form

$$\frac{1}{\sqrt{2}}(\alpha\alpha\alpha\beta\beta\beta - \beta\beta\beta\alpha\alpha\alpha) \tag{3}$$

This is one of five spin eigenfunctions[29] (SEF) for six electrons coupled into a singlet state. Provided that the spatial orbitals multiplying this SEF are ordered such that orbitals localised on each Mn ion are grouped together, we expect this SEF to dominate the CI wave function, since Hund's rule requires spins on each ion to be coupled with the same spin. This is indeed found to be the case in the actual CI wave function for the singlet state of the $Mn_2O_{11}^{14-}$ cluster representing $CaMnO_3$. The wave function for the singlet state is therefore

$$\psi^{singlet} = \frac{1}{\sqrt{2}}A\Big(\{core\}(\phi_{xy,l}\phi_{xz,l}\phi_{yz,l}\phi_{xy,r}\phi_{xz,r}\phi_{yz,r})(\alpha\alpha\alpha\beta\beta\beta - \beta\beta\beta\alpha\alpha\alpha)\Big) \tag{4}$$

Using conventional rules for evaluating determinantal energies[33], the energy difference between the two states is $K_{xz,l\ xz,r} + K_{yz,l\ yz,r}$, with the singlet state lying *above* the septet state (assuming that other inter-site exchange integrals are zero because of negligible spatial overlap). When the ground state energies of the singlet and septet states of the $Mn_2O_{11}^{14-}$ cluster with wave functions in Eq. 2 and 4 were evaluated, the singlet state was 3.6 meV above the septet state. This implies a value of 1.8 meV for the exchange integrals just mentioned. Note that we use the notation K_{ij} for exchange integrals between specific molecular orbitals while we use the notation J for the (effective) exchange coupling energy of two spins on different Mn ions. The singlet and septet states of this configuration are analogous to the Heitler-London valence bond wave function for the singlet and triplet states of the He atom in a 1s2s configuration. In that case the triplet state is lower than the singlet state by K_{1s2s}.

In general, CI wave functions with N electrons in the active orbital space consist of linear combinations of spin-adapted functions (SAF's)

$$\psi_{CI} = \sum_i c_i\ \psi_i^{SAF} \tag{5}$$

$$\psi_i^{SAF} = A\Big(\{core\}\phi_j\phi_k...\phi_s\phi_t\Theta_a\Big) \tag{6}$$

where a SAF is a product of spatial orbitals and a SEF, Θ_a, for the particular spin state in question. The septet and singlet SAF's in Eq. 2 and 4 are the dominant terms in a more general CI expansion of the septet and singlet wave function of the $Mn_2O_{11}^{14-}$ cluster. All SAF's which are obtainable by exciting one or two electrons from the dominant SAF's to empty orbitals in the active space are included in the expansion. As stated above, the 13 orbitals in the active space in the calculations described here are comprised of 10 orbitals of mainly Mn 3d character and 3 of mainly O 2p character localised on the O ion between the two Mn ions. These excited electron SAF's enter the wave function with a maximum weight of order 10^{-2} and a corresponding occupancy of order 10^{-4} and it is these which lower the energy of the singlet state below the septet state when the spins are AF coupled. The main excited SAF's in the singlet and septet wave functions are those in which: *one* electron is excited from an O 2p orbital to the Mn e_g orbital aligned with the Mn-O axis (O to e_g (1e)); a *pair* of electrons are excited from one O 2p orbital to the *same* Mn e_g orbital (O to e_g (2e)) and an excitation in which a t_{2g} electron is transferred fron one Mn ion to the other (t_{2g} exchange). Obviously the latter exchange process is only allowed in the singlet state as it violates the Pauli exclusion principle in the septet state when the t_{2g} shells are half filled, as in $CaMnO_3$. Excitations in which a pair of electrons are excited from the O ion to separate Mn ions are found to have negligible weight for both spin states.

III. RESULTS

A. $CaMnO_3$: Bulk UHF Calculations

UHF total energy calculations were performed using the CRYSTAL98 code[34] for FM, A-, C-, and G-AF spin orderings. The energy of the cubic FM structure with the experimental lattice constant of 3.73 Å was adopted as the reference energy (0 meV); calculations were also performed for each of the spin orderings with a lattice constant of 3.75 Å. Total energies and magnetic moments from these calculations are given in Table I. When these total energy differences are fitted to the Hamiltonian in Eq. 1 with nearest (J_1) and second nearest (J_2) neighbour interactions (*i.e.* along [a,0,0] and [a,a,0], where a is the lattice constant), the parameters obtained for a lattice constant of 3.73 Å are $J_1 = 10.7$ meV, $J_2 = 0.3$ meV and for a lattice constant of 3.75 Å, the parameters are $J_1 = 10.1$ meV, $J_2 = 0.3$ meV. It is generally believed that exchange interactions which connect magnetic ions along a linear chain are stronger than those which do not, such as the J_2 interaction here. However, in the cubic perovskite structure, exchange interactions along [2a,0,0], *etc.* contribute equally to all four spin orderings studied and so cannot be extracted from the data presented here. Similar values for J_1 have been obtained from model Hamiltonian calculations by Meskine *et al.* ($J_1 = 9.5$ meV)[8]. Note that the definition used for the exchange energy in that work, the difference between the energy of a pair of ferro- and anti-ferromagnetically coupled Mn ions, is *twice* the exchange energy defined in Eq. 1 above. Hence values for exchange energies from that work have been divided by two in order to compare them to values in the present work.

B. $CaMnO_3$: Cluster CI Calculations

Exchange energies obtained from cluster CI calculations depend strongly on Mn e_g and O 2p orbital populations. In turn these populations depend on the Madelung potential of a sphere of point charges surrounding the $Mn_2O_{11}^{14-}$ cluster. The charges were located on crystal ion sites and Mulliken populations of ions in bulk UHF calculations on $CaMnO_3$ were used as a guide in choosing the magnitudes of these charges. The sphere of point charges had a radius of just over 20 Å and contained around 3300 charges. The radius was chosen so that the sphere was overall almost charge neutral; each unit cell of point charges was also neutral. The dependence of exchange energies in $CaMnO_3$ and $LaMnO_3$ on Mn ion charge, measured by the Mulliken population of that ion in the SCF cluster calculation, is shown in Fig. 5. The charge on the two Mn ions *in the cluster* was adjusted by transferring charge from Mn point charge sites to Ca or La point charge sites *in the sphere of point charges*. The total charge of the Mn and Ca (or La) point charges was kept constant and the O ion charge was maintained at the UHF Mulliken population value. It can be seen that the magnitude of the exchange energy increases as charge is removed from the Mn ion, which is reasonable as charge is mainly being transferred to/from the e_g orbitals which are directly involved in the exchange coupling mechanism - as the e_g orbital becomes filled, the exchange energy diminishes. The CI calculation value of $J_1 = 8.1$ meV quoted for $CaMnO_3$ in Table II is the value obtained for an Mn cluster ion charge of +2.13, the Mn ion charge determined from the UHF calculation. This is to be compared to an estimate of the experimental value of $J_1 = 6.6$ meV, derived from the Néel temperature of $CaMnO_3$.

The fundamental SAF's for the septet and singlet states of the $Mn_2O_{11}^{14-}$ cluster were given in Eq. 2 and 4. In the fundamental SAF wave functions for either spin state, each has a SAF coefficient, c_i, of unity, however when additional SAF's are permitted in the wave function (*i.e.* permitting O^{2-} ion 2p to e_g excitations, *etc.*) the weights of fundamental SAF's are around 0.9950 and additional SAF's corresponding to O superexchange and t_{2g} exchange enter the wave function with SAF coefficients of order 0.01. Even for limited active spaces (as in these calculations) the number of SAF's entering the wavefunction means that a convenient way to analyse the wavefunction is to tabulate the summed occupancies (*i.e.* $\mid c_i^2 \mid$) of configurations of a particular type. There are, for example, several SAF's in which one electron is excited from an O 2p orbital to an Mn e_g orbital[35]. The relative magnitudes of these occupancies are a measure of the importance of each type of fluctuation about the fundamental SAF configurations. Summed occupation numbers for the $Mn_2O_{11}^{14-}$ cluster are given in Table III. It can be seen that the fundamental (or main) SAF has occupancy 0.9926 for the singlet state while it has occupancy 0.9943 in the septet state and therefore that there are larger correlation effects in the singlet state. SAF's in which a t_{2g} electron has hopped from one Mn ion to the other have an occupancy of 0.0005, while these fluctuations are absent from the septet state owing to the Pauli exclusion principle, as noted above. However, the main difference in septet and singlet wave functions is in the occupancy of states in which one electron is transferred from an O 2p orbital to an e_g orbital, the occupancy being 0.0038 for the singlet state and 0.0027 for the septet state. The occupancy of SAF's in which a pair of electrons is transferred from O 2p to one Mn e_g orbital is the same for both spin states. The energies of both spin states relative to the energy of the fundamental septet SAF are also given in Table III. The septet state with O superexchange fluctuations is 133.4

meV below the fundamental septet SAF. This is the correlation energy for that state[36]. The singlet state with O superexchange and t_{2g} fluctuations is 149.6 meV below the reference energy and 153.2 meV below the fundamental singlet SAF energy. The latter energy is the correlation energy for the singlet state. Correlation energies for the $Mn_2O_{11}^{14-}$ and $Mn_2O_{11}^{16-}$ cluster CI wave functions are illustrated schematically in Figure 6. Correlation energies are around 50 percent larger in $Mn_2O_{11}^{14-}$ than in $Mn_2O_{11}^{16-}$ and this is reflected in the larger exchange energy in $CaMnO_3$. It is worth noting that when the CI cluster calculation for the exchange energy in $CaMnO_3$ was performed with no point charge array surrounding the cluster, the exchange energy obtained was 57 meV, well in excess of the experimental value. This emphasises the importance of Madelung terms in the crystal Hamiltonian in determining exchange energies in strongly correlated materials.

C. $LaMnO_3$: Bulk UHF Calculations

Total energy calculations were performed on $LaMnO_3$ in the ideal perovskite (cubic) structure, a tetragonal perovskite structure, a cubic structure with a Jahn-Teller distortion of the MnO_6 octahedra and the *Pnma* structure with atomic coordinates derived from experiment[18] and by minimising the total energy by varying lattice parameters and internal coordinates not determined by symmetry. These structures are summarised in Table IV. The Jahn-Teller distortion consisted of elongation or contraction of Mn-O bonds parallel to the *ac* axes of the unit cell. These are the Mn-O bonds which induce FM coupling between Mn ions in the *Pnma* structure. The cubic structure with the lowest energy had a lattice constant of 3.953 Å (volume 61.77 $Å^3$ per Mn ion) which is comparable to the lattice constant of the 'cubic' phase of $LaMnO_3$ (3.947 Å) which occurs at temperatures above 750K[17]. All relative energies and lattice volumes will be assumed to be per Mn ion hereafter. When this structure is changed by a 5 percent Jahn-Teller distortion (Table IV) the energy is lowered by 304 meV and the magnetic ground state of the structure switches from $d_{x^2-y^2}$ $d_{3z^2-r^2}$ FM to $d_{3x^2-r^2}$ $d_{3y^2-r^2}$ FM (see below).

The total energy of the *Pnma* structure using coordinates from experiment[18] (Table IV) is 200 meV above the Jahn-Teller distorted structure. The total energy of the *Pnma* structure was minimised[37] by varying the lattice parameters and 7 internal coordinates not determined by symmetry of the *Pnma* space group. The total energy of the energy minimised structure is 6 meV above the Jahn-Teller distorted structure. The optimised lattice parameters and internal coordinates are given in Table IV; the *a* lattice vector is essentially unchanged while the *b* and *c* lattice vectors increase in magnitude by 1.1 and 1.6 percent, respectively. The lattice volume rises from 60.89 to 62.53 $Å^3$. Probably the most important changes which occur on minimising the total energy are: the degree of Jahn-Teller distortion is reduced; La-O distances increase significantly. In the lowest energy cubic structure there is one Mn-O distance of 1.976 Å and an La-O distance of 2.795 Å. On introducing the 5 percent Jahn-Teller distortion these become Mn-O distances of 1.877, 1.976 and 2.075 Å and La-O distances of 2.795 and 2.797 Å. In the experimental *Pnma* structure[18] the Mn-O distances are 1.903, 1.957 and 2.185 Å and the La-O distances are 2.433, 2.461 and 2.548 Å. These change to 1.910, 1.944 and 2.135 Å and 2.609, 2.666 and 2.684 Å in the energy minimised structure. Hence lower energies are found for structures with larger La-O distances and a

reduced Jahn-Teller distortion. The combined ionic radii of La^{3+} and O^{2-} are 2.76 Å[38]. La-O distances in the energy minimised *Pnma* and cubic structures lie just below the combined ionic radii distance, whereas the La-O distances in the experimental *Pnma* structure lie well below this distance. The cubic structure with a Jahn-Teller distortion and the energy minimised *Pnma* structure are both lower in energy than the lowest energy cubic structure by around 300 meV. This energy lowering by a Jahn-Teller distortion is half of the lowering assumed by Millis[39] in a calculation of electron-phonon coupling in $Ca_{1-x}La_xMnO_3$. The UHF calculations reported here are similar to those reported by Su *et al.*[15]. They report an energy lowering of 1055 meV when the cubic structure is changed to the experimental *Pnma* structure with no volume change. This calculation will overestimate the energy difference between such structures as the cubic structure with the *Pnma* structure equilibrium volume is not the mimimum energy cubic structure.

For the cubic perovskite structure it was found that variations of the total energies of different spin and orbital orderings can be fitted very well by a Hamiltonian of the form

$$H = \sum_{<ij>} J_{ij} \frac{\hat{S}_i . \hat{S}_j}{S^2} + H_{OO} \tag{7}$$

where H_{OO} is an orbital ordering term which depends only on the orbital order. For these calculations the cubic unit cell was doubled along [110], [101] and [011] directions (G-AF spin and orbital ordering) and along the [001] direction (A-AF spin and orbital ordering) and total energies and charge density difference plots[40] were computed for $d_{x^2-y^2}$ $d_{x^2-y^2}$, $d_{x^2-y^2}$ $d_{3z^2-r^2}$ and $d_{3z^2-r^2}$ $d_{3z^2-r^2}$ orbital orderings and FM, A-AF and G-AF spin orderings. The $d_{x^2-y^2}$ $d_{3z^2-r^2}$ A-AF combination is incompatible with the unit cell doublings chosen and was omitted. Total energies are given in Table V and charge density difference plots for each of these orbital orderings are shown in Fig. 7.

For $d_{x^2-y^2}$ $d_{x^2-y^2}$ and $d_{3z^2-r^2}$ $d_{3z^2-r^2}$ orbital ordering, distinct exchange constants in the xy plane, $J_\parallel$, and in the xz plane, $J_\perp$, are postulated, whereas for $d_{x^2-y^2}$ $d_{3z^2-r^2}$ ordering a single exchange constant, $J = J_\parallel = J_\perp$, is postulated. Exchange constants for each orbital ordering are given in Table VI. AF exchange constants are obtained when adjacent Mn orbital ordering is the same and FM coupling is observed when adjacent Mn e_g orbitals differ. This observation also applies to *Pnma* structures studied: FM coupling is observed between in-plane Mn ions with alternating e_g orbital orientations; AF coupling is observed when adjacent Mn e_g orbitals have the same orientation. Magnitudes of AF couplings vary between 5.1 and 14.2 meV and one FM coupling of -6.0 meV is observed in the $d_{x^2-y^2}$ $d_{3z^2-r^2}$ A-AF ordering.

Once exchange constants have been computed for a particular orbital ordering, comparison of structures with the same magnetic structure but different orbital ordering permits differences in orbital ordering energies to be calculated. The actual magnitude of orbital ordering energy, H_{OO}, of course depends on the reference energy chosen. The choice of the FM $d_{x^2-y^2}$ $d_{x^2-y^2}$ structure as the reference energy structure yields values of -17.4, -20.0 and -113.4 meV for the $d_{x^2-y^2}$ $d_{x^2-y^2}$, $d_{3z^2-r^2}$ $d_{3z^2-r^2}$ and $d_{x^2-y^2}$ $d_{3z^2-r^2}$ relative orbital ordering energies. The important result here is that an alternating orbital order ($d_{x^2-y^2}$ $d_{3z^2-r^2}$) is around 90 meV below those with the same orbital order on each site ($d_{x^2-y^2}$ $d_{x^2-y^2}$ or $d_{3z^2-r^2}$ $d_{3z^2-r^2}$) in the cubic perovskite structure. When the values of H_{OO} and exchange

constants just mentioned are used to compute the relative energies of the eight spin and orbital orderings considered, the maximum deviation from the relative energies reported in Table IV is 0.2 meV, demonstrating the suitability of the Hamiltonian in Eq. 7. The fact that charge density difference plots for different spin ordering and the same orbital ordering are very similar suggests that this should be the case.

Using the fact that orbital and spin contributions to the Hamiltonian are independent, differences in total energy of a particular spin order as a function of lattice distortion may be attributed to differences in orbital ordering energy. Fig. 8 is a plot of total energy for each orbital ordering with G-AF magnetic order as a function of isovolume, tetragonal lattice distortion. These calculations were performed using P4/mmm space group symmetry. It can be seen that $d_{x^2-y^2}$ $d_{3z^2-r^2}$ orbital ordering is the most stable ordering only within a small parameter range about the cubic structure. When the tetragonal distortion is such that the lattice is elongated along the z axis, $d_{3z^2-r^2}$ $d_{3z^2-r^2}$ ordering is favoured and when it is compressed along this axis, $d_{x^2-y^2}$ $d_{x^2-y^2}$ ordering is favoured. This may be explained by a simple electrostatic argument - the ordering which is favoured in either case is the one where the occupied e_g orbitals are oriented along the elongated axis or axes, thereby reducing the Coulombic repulsion energy. The greatest stabilisation relative to the cubic lattice is found for an x/z ratio of 0.94 where the energy is 164 meV below that of the cubic G-AF reference energy. This stabilisation is still significantly less than the stabilisation of 298 meV which results when the energy minimised *Pnma* structure is adopted.

Relative energies and exchange constants for the Jahn-Teller distorted structure and both *Pnma* structures studied are given in Tables VII and VIII, respectively. Charge density difference plots for the Jahn-Teller distorted and energy minimised *Pnma* structures are shown in Fig. 9. The magnetic ground state of the Jahn-Teller distorted structure is FM, but this is almost isoenergetic with the A-AF structure. This is because the in-plane exchange constant is FM while the out-of-plane exchange constant is FM (but small). The magnetic ground state of the cubic structure is G-AF with AF coupling between all neighbouring Mn ions. The switch to FM coupling between neighbouring Mn ions in-plane is due to the Jahn-Teller distortion in-plane. Both *Pnma* structures studied have A-AF magnetic ground states (as is the case in nature) but magnitudes of exchange constants obtained from these calculations are smaller than those obtained from neutron scattering data[2,3] (Table VIII). Values of 0.6 and -3.7 meV for $J_\perp$ and $J_\parallel$ may be compared to 0.8 and -3.5 meV obtained in a similar UHF calculation[15] and 4.8 and -6.7 meV from experiment[2,3]. A local spin density approximation (LSDA) calculation[11] found values of -3.1 and -9.1 meV for $J_\perp$ and $J_\parallel$. This calculation did find an A-AF ground state for *Pnma* $LaMnO_3$, however, as second nearest neighbour exchange constants are significant in the LSDA calculation and favour an A-AF magnetic ground state.

D. $LaMnO_3$: Cluster CI Calculations

Cluster CI calculations for $LaMnO_3$ were performed using $Mn_2O_{11}^{16-}$ clusters with the Mn ions in the same configuration as a pair of Mn ions in the *ac* plane (Fig. 1) and with the Mn ions along a line parallel to the *b* axis. The former cluster corresponds to a pair of Mn ions which is expected to be FM coupled while the latter corresponds to a pair of

ions which is expected to be AF coupled. Mn e_g orbital ordering in the former cluster had the form illustrated schematically in Fig. 2c while the latter had orbital ordering as in Fig 2b. Clusters and surrounding point charges with the experimental *Pnma* structure[18] and the energy minimised structure were used. Exchange constants for $LaMnO_3$ derived from these cluster calculations are given in Table VIII. Cluster CI calculations with Mn, O and La surrounding point charges of 2.6, -1.8 and 2.8 (close to Mulliken population values from UHF calculations) result in exchange constants of 3.3 and -3.6 meV for $J_\perp$ and $J_\parallel$ when the experimental structure is used. These values change to 5.1 and -7.4 meV when the energy minimised structure (Table IV) is used.

The Madelung potential has an important role in determining exchange constants in manganites. Obviously ions several lattice constants or more distant from the ions in the central cluster may be treated as point charges rather than distributed charges without significantly altering the potential within the central cluster. However point charges adjacent to the central cluster may cause a significantly different potential within the cluster and affect the results of the exchange constant calculation. This question has previously been addressed by other workers[25,27]. In order to estimate the effect of terminating the cluster with point charges, cluster CI calculations were performed with the 12 La point charges nearest to the central cluster ions replaced by La^{3+} pseudopotentials[41]. This resulted in a small increase in $J_\perp$ and no change in $J_\parallel$ compared to the calculation where only point charges were used. The values obtained for $J_\perp$ and $J_\parallel$ from these calculations were 5.2 and -7.4 meV, which are in good agreement with the experimental values: 4.8 and -6.7 meV. Values for the exchange constants derived from the model Hamiltonian calculations of Meskine *et al.*[8] are also given in Table VIII.

Relative energies and SAF occupancies for the $Mn_2O_{11}^{16-}$ clusters used for calculating exchange constants in $LaMnO_3$ in the energy minimised structure are given in Table IX. The fundamental SAF singlet states are 11.9 meV ($J_\perp$) and 17.9 meV ($J_\parallel$) above the nonet states of the clusters. When additional SAF's are permitted in the wave function the singlet(nonet) states are lowered by 105.4(83.3) meV ($J_\perp$) and 82.8(79.7) meV ($J_\parallel$). These are the correlation energies for these states. The singlet state of the cluster used to calculate $J_\perp$ is 10.2 meV lower in energy than the nonet state giving a value for $J_\perp$ of 5.1 meV while the nonet state of the cluster used to calculate $J_\parallel$ is 14.7 meV lower in energy than the singlet state giving a value of -7.4 meV for $J_\parallel$. From Table IX it can be seen that O to e_g (1e) excitations are the main fluctuations about the fundamental SAF state. The weight of the fundamental SAF in the singlet states of either cluster is less than in the nonet states, reflecting the greater degree of correlation in the singlet states. In the $J_\perp$ calculation the greater correlation energy of the singlet state *c.f.* the nonet state is sufficient to make the singlet state the ground state and give an AF exchange constant. On the other hand, in the $J_\parallel$ calculation the singlet correlation energy is just greater than that of the nonet state and, together with the fact that the singlet state of the fundamental SAF wave function is 17.9 meV above the nonet state, this results in a nonet ground state and an FM exchange constant.

IV. DISCUSSION

UHF and CI cluster calculations for the exchange constant in $CaMnO_3$ are in reasonable agreement with estimates for its value based on the Rushbrooke-Wood formula[5] and its Néel temperature. The calculated exchange constants are larger than the estimate based on experiment. The single AF exchange constant is mainly a result of O to e_g (1e) excitations which lower the energy of the singlet state of a pair of adjacent Mn ions below that of the septet state. The magnitude of the exchange constant derived from CI cluster calculations depends strongly on the Madelung potential within the cluster and there is agreement between theory and estimates based on experiment only when that potential results in ionic charges in the cluster similar to those in the bulk UHF calculation.

$LaMnO_3$ is more complex than $CaMnO_3$. It is also more ionic than $CaMnO_3$ with Mulliken populations of ions closer to the formal ion charges. A number of orbital and spin ordered states exist within a small energy range, say 300 meV, close to the ground state. The energies of several spin and orbital ordered states of cubic $LaMnO_3$ are well described by the Hamiltonian in Eq. 7. In the remainder of this section exchange constants in cubic and Jahn-Teller distorted $LaMnO_3$ are correlated with Mn^{3+} ion orbital ordering and O^{2-} ion charge density distortions and Mn^{3+} ion interactions are identified as type I, II or III according to Goodenough's scheme[24]. Finally, the role of correlation and availability of empty orbitals on magnetic ion sites in AF and FM coupling is discussed.

Cubic $LaMnO_3$ has a $d_{x^2-y^2}$ $d_{3z^2-r^2}$ FM ground state and a lattice constant of 3.953 Å. Exchange constants depend on orbital ordering and range from -6.0 to 14.2 meV. Charge density difference plots (Fig. 7) show that the charge density on an Mn ion is essentially independent of charge densities on neighbouring ions. That density is determined solely by the ion's orbital ordering. However, charge densities on more polarisable O^{2-} ion sites depend on charge densities at both neighbouring Mn ion sites. For $d_{3z^2-r^2}$ $d_{3z^2-r^2}$ orbital ordering (Fig. 7, top panels), O^{2-} ions in Mn-O bonds in the xy plane undergo a quadrupolar distortion in which charge is displaced from the Mn-O bond axis into directions perpendicular to the bond while O^{2-} ions in Mn-O bonds along the z axis are much less severly distorted and the ions tend to elongate along the bond axes. The $d_{3z^2-r^2}$ character of the ordered Mn e_g orbitals can be seen clearly in the top right panel of Fig. 7. The exchange constant for Mn^{3+} ions in the xy plane with this orbital ordering is $J_{\parallel}$ = -0.1 meV while the exchange constant for Mn^{3+} ions along the z axis is 14.2 meV. Thus a weak exchange coupling is associated with the quadrupolar distortion of charge away from the bond axis while a much stronger coupling is associated with a nearly spherical ion in which charge density tends to concentrate along the bond axis, compared to the spherical O^{2-} ion.

For $d_{x^2-y^2}$ $d_{x^2-y^2}$ orbital ordering the $d_{x^2-y^2}$ character of the ordered Mn e_g orbitals is clearly seen in the middle left panel of Fig. 7. There is a relatively weak quadrupolar distortion of the O^{2-} ions in the xy plane and a stronger quadrupolar distortion of O^{2-} ions along the z axis. The exchange constant for Mn^{3+} ions in the xy plane is 5.1 meV while it is 7.2 meV for Mn^{3+} ions along the z axis.

The $d_{x^2-y^2}$ or $d_{3z^2-r^2}$ character of orbital ordering can be seen in both bottom panels in Fig. 7. In the xy and xz planes the O^{2-} ion charge density is polarised in a circulating pattern, even though the O^{2-} ions are situated midway between the Mn^{3+} ions. Charge is polarised towards regions at Mn^{3+} ion sites where there is a reduction in charge density

below that of spherical Mn^{4+} ions, as indicated by negative contours in the charge density difference plots. Around each Mn^{3+} ion with the $d_{3z^2-r^2}$ e_g orbital occupied, charge is deformed towards the $d_{3z^2-r^2}$ ion in the xy plane and away from it along the z axis, whereas for Mn^{3+} ions with the $d_{x^2-y^2}$ e_g orbital occupied, charge is deformed towards it along the z axis and away from it in the xy plane. Thus each Mn^{3+} ion is coupled to each neighbouring Mn^{3+} ion by a polarised O^{2-} ion and there is one FM exchange constant of -6.0 meV.

A simple pattern of orbital ordering is obtained for the Jahn-Teller distorted structure where the unit cell was doubled in the [001] direction (Fig. 9). This pattern of orbital ordering was obtained without biasing the initial guess wave function in anyway (Appendix A). Orbital ordering in the xy plane is an alternating $d_{3x^2-r^2}$ $d_{3y^2-r^2}$ pattern which is repeated with period one along the z axis. This is the a-type orbital ordering discussed in Ref.[42]. The FM exchange constant between Mn^{3+} ions in the xy plane is -8.1 meV and the weak FM exchange constant along the z axis is -0.1 meV. There is strong deformation of O^{2-} ion charge density in the xy plane towards regions of reduced charge density at the Mn^{3+} ion sites, associated with strong FM exchange coupling (Fig. 9, left panel). There is strong quadrupolar distortion of the charge density at O^{2-} ion sites coupling Mn^{3+} ions along the z axis, associated with a weak FM exchange coupling.

The same a-type orbital ordering is also found in the *Pnma* structures studied. There is a similar pattern of circulating charge polarisation towards regions at Mn^{3+} ion sites where the charge density is reduced and there is strong FM exchange coupling between Mn^{3+} ions lying approximately in the ac plane (-3.7 and -6.0 meV, UHF calculations Table VIII).

The three Mn-Mn interactions described by Goodenough[24] are now tentatively identified in cubic and Jahn-Teller distorted $LaMnO_3$ using charge densities on the O^{2-} sites and orbital ordering at the neighbouring Mn ion sites. Type I interactions are found for: $d_{x^2-y^2}$ $d_{x^2-y^2}$ orbital ordering in cubic $LaMnO_3$ for both $J_{\parallel} = 5.1$ meV and $J_{\perp} = 7.2$ meV (Fig. 7, middle panels); $d_{3z^2-r^2}$ $d_{3z^2-r^2}$ orbital ordering for $J_{\perp} = 14.2$ meV (Fig. 7, top right panel).

Type II interactions are found for: $d_{x^2-y^2}$ $d_{3z^2-r^2}$ orbital ordering in cubic $LaMnO_3$ (Fig. 7, bottom panels) for both $J_{\perp}$ and $J_{\parallel}$ = -6.0 meV; $d_{3x^2-r^2}$ $d_{3y^2-r^2}$ orbital ordering in Jahn-Teller distorted $LaMnO_3$ (Fig. 9, left panel ($J_{\parallel}$ = -8.1 meV). Charge densities are characterised by breaking of symmetry of the O^{2-} ion along the Mn-O-Mn axis. Obviously this can only occur when the orbital orderings on adjacent Mn ions differ, however this observation is worth making as such symmetry breaking is characteristic of FM exchange coupling.

Type III interactions are found for $d_{3z^2-r^2}$ $d_{3z^2-r^2}$ orbital order in cubic $LaMnO_3$ (Fig. 7, top left panel) where $J_{\parallel}$ = -0.1 meV; for $J_{\perp}$ =-0.6 meV in the Jahn-Teller distorted structure (Fig. 9, right panel). In both cases the weak exchange coupling is associated with strong, quadrupolar O^{2-} charge density deformation.

Cluster CI calculations provide detailed information on the exchange coupling mechanism. Fundamental SAF singlet states for clusters representing both $CaMnO_3$ and $LaMnO_3$ lie above the fundamental SAF high spin multiplicity states; this is expected to be the case for a wide range of magnetic ions exchange coupled *via* a closed shell anion. The ground state for the pair of magnetic ions is AF when the *difference* in correlation energies of the singlet and high spin multiplicity states exceeds the singlet/high spin state splitting, otherwise it is FM. Correlation energies for singlet states exceed correlation energies of the corresponding high spin multiplicity states in the three cases studied here (Fig. 6). This is also likely to be

true for a wide range of magnetic ions which are exchange coupled *via* a closed shell anion as there are many more singlet SAF's than high spin SAF's in any particular active space. For example, in the active space used for the $LaMnO_3$ cluster CI calculations there are over 18,000 singlet SAF's compared to over 1,500 nonet SAF's, which simply reflects the fact that there are many more ways to arrange spin-coupled electrons to form singlet states than there are to form nonet states for a specific number of electrons. Only a few of either the singlet or nonet SAF's appear in the ground state wave functions with a signicant weight, but since there are so many more singlet than nonet SAF's, it is not surprising that the singlet state correlation energy is larger.

When one empty Mn e_g orbital is available to accept one or two electrons from an O^{2-} ion, as is the case for $J_{\parallel}$ in *Pnma* $LaMnO_3$, the singlet state correlation energy is only slightly larger than the nonet state correlation energy (82.8 versus 79.7 meV) and the nonet state is the ground state. However, when two empty Mn e_g orbitals are available, as is the case for $J_{\perp}$ in *Pnma* $LaMnO_3$ and J in $CaMnO_3$ (Fig. 6), singlet state correlation energies are significantly larger than the nonet(septet) state correlation energies (105.4 versus 83.3 meV ($LaMnO_3$) and 153.2 versus 133.4 meV ($CaMnO_3$)) and the ground states are singlets.

Exchange coupling in $CaMnO_3$ and $LaMnO_3$ is largely due to quantum fluctuations in the ground state in which one electron is excited from an O^{2-} ion into an Mn e_g orbital. Fluctuations in which an electron is exchanged between t_{2g} orbitals enter the singlet state in $Mn_2O_{11}^{14-}$ and $Mn_2O_{11}^{16-}$ clusters but are not the main contributors to the exchange interaction. Parallel studies of exchange coupling in La_2CuO_4[43] show that $d_{x^2-y^2}$ $d_{x^2-y^2}$ exchange interactions dominate the exchange coupling in La_2CuO_4 and O to $d_{x^2-y^2}$ excitations have a lesser weight than $Cu^{1+}Cu^{3+}$ excitations in the La_2CuO_4 ground state. This difference in exchange coupling mechanism most likely reflects trends in effective Hubbard U parameters for $Mn^{3+/4+}$ and Cu^{2+} and O 2p to metal d excitation energies.

ACKNOWLEDGMENTS

This work was supported by Enterprise Ireland under grant number SC/00/267. M. N. wishes to acknowledge support by the Trinity Trust.

APPENDIX A: DETAILS OF CALCULATIONS

The methods used to generate localised orbitals and point charge arrays and the basis sets and CI computer codes used in this work are described in this section.

UHF calculations on the crystalline solid were performed using the CRYSTAL98 code[34]. The basis sets used for both crystal UHF calculations and cluster CI calculations were identical Gaussian orbital basis sets designed for use in the solid state. They are slightly modified versions of the basis sets available from the CRYSTAL98 website[44]. Outer exponents of the Gaussian functions were modified so that the total energy in a UHF calculation on $CaMnO_3$ was minimised. The original basis sets had been optimised for different Mn ionic solids. The basis sets used in all calculations are the all electron basis sets for: Mn (86-411d41G[45] with two d orbital exponents, optimised for $CaMnO_3$ by changing the outer d exponent to 0.259); O (8-411G[45] with principal quantum number up to n = 4, optimised

for $CaMnO_3$ by changing the outer sp exponents to 0.4763 and 0.22); Ca (86-511d3G[46] with the outer d orbital exponents optimised for $CaMnO_3$ to 3.191, 0.8683 and 0.3191) and an La basis set optimised for the La^{3+} ion[48]. The La basis set used in this work differs from the cited basis in that the 5d orbital was removed from the basis and the 6sp and 7sp orbitals were replaced by a single sp orbital exponent of 0.3917.

Different orbital ordered states in UHF calculations were obtained using a feature in the CRYSTAL98 code which increases the diagonal element of the Fock matrix corresponding to a particular orbital for the first few iterations of the calculation. This results in that orbital being unoccupied during those SCF cycles and allows the wave function to converge to a state which is a local energy minimum with a particular orbital ordering.

High spin multiplicity states, such as the septet and nonet states of the clusters used here, are generally well described by a self consistent field (SCF) restricted open shell Hartree-Fock (ROHF) wave function. All electrons on the cluster were treated explicitly - no pseudopotential approximation was used, except in the test calculation with a La^{3+} pseudopotential described above. CI calculations were performed in localised orbital bases, rather than the canonical molecular orbital bases derived from the SCF ROHF calculations. Localisation of SCF ROHF molecular orbitals was performed using the Foster-Boys algorithm[47], which generates localised orbitals with maximally separated centroids. Doubly occupied O 2p orbitals, singly occupied Mn t_{2g} (or t_{2g} and an e_g orbital for $Mn_2O_{11}^{16-}$) orbitals and unoccupied Mn e_g orbitals were localised in three separate localisation steps. These must be performed separately in order to preserve invariance of the ROHF total energy, since any mixing between orbitals of different occupancy will increase the total energy. In the localised orbital ROHF wave functions for either spin state of the $Mn_2O_{11}^{14-}$ and $Mn_2O_{11}^{16-}$ clusters, each Mn d electron occupies a separate orbital.

Calculations on low spin multiplicity states of the clusters used the same sets of localised orbitals. They demonstrate that the localised orbitals generated for the high spin multiplicity states are very good approximations to the optimal orbitals for open shell low spin multiplicity states and that a high spin multiplicity ROHF wave function ought to be an excellent starting point for perturbative calculations on high and low spin multiplicity states in the solid state.

In a CI calculation on a cluster of this size it is essential to partition the orbital space into a core space (with doubly occupied orbitals), an active space of orbitals which are occupied or unoccupied in the ROHF main configuration and a space of redundant, unoccupied orbitals which are not used in the calculation. The active orbitals in this work were the three O 2p localised orbitals on the central O^{2-} and a set of t_{2g} and e_g orbitals on each Mn ion. The Direct Multi-Reference CI module[31] in the GAMESS[28] programme was used for this work. The active space consisted of either the (single) fundamental SAF orbitals or the fundamental SAF plus all possible single or double excitations which can be made from the fundamental SAF into empty active space orbitals.

Calculations were performed for clusters with no surrounding point charges and with point charges in a spherical volume surrounding the cluster. The radius of the sphere was over 20 Å and included around 3300 charges. The charges were located on the ionic sites of either $CaMnO_3$ or $LaMnO_3$. Mulliken populations derived from UHF crystal calculations were used as guides for point charge magnitudes. For $CaMnO_3$, UHF Mulliken populations were $Ca^{+1.86}Mn^{+2.13}O_3^{-1.33}$. However, in the SCF ROHF cluster calculation, this choice

of point charges results in Mulliken populations of $Mn^{+2.60}O^{-1.31}Mn^{+2.60}$ on the central Mn-O-Mn chain in the cluster. The Mn and Ca point charge magnitudes were adjusted to $Ca^{1.15}Mn^{2.84}O^{-1.33}$ and this resulted in Mulliken populations of $Mn^{+2.17}O^{-1.61}Mn^{+2.17}$ on the central Mn-O-Mn chain and populations of -1.64 and -1.67 on the other two O types in the cluster. Note that this adjustment leaves each point charge unit cell charge neutral and the point charge sphere radius is adjusted so that the entire cluster has a charge near zero. The major changes which occur on adjusting the point charges are: charge is transferred from the outer O ions in the cluster to the Mn ions and central O ion, each gaining about 0.4e; the AF exchange constant changes from 21.0 meV to 8.1 meV, in agreement with other calculation methods and in reasonable agreement with experiment; the degree of correlation in the wavefunction decreases sharply. When a $Mn_2O_{11}^{14-}$ cluster with no external point charges is used, the Mulliken populations on the central Mn-O-Mn chain are $Mn^{+2.46}O^{-0.94}Mn^{+2.46}$ and the exchange coupling energy is 57 meV.

A similar adjustment of point charge magnitudes was used for the $Mn_2O_{11}^{16-}$ cluster CI calculations. The Mulliken populations determined from UHF crystal calculations on the experimental *Pnma* structure were $La^{+3.15}O^{-1.75,-1.82}Mn^{+2.24}$. Cluster point charges of $La^{+2.80}O^{-1.80,-1.80}Mn^{+2.60}$ resulted in Mulliken populations of $Mn^{+2.45}O^{-1.65}$ in the *Pnma* structure.

REFERENCES

[1] J. M. D. Coey, M. Viret and S. von Molnár, Adv. Phys. **48** , 167 (1999).
[2] K. Hirota, N. Kaneko, A. Nishizawa and Y. Endoh, J. Phys. Soc. Jpn. **65**, 3736 (1996).
[3] F. Moussa, M. Hennion, J. Rodriguez-Carvajal, M. Houdden, L. Pinsard, A. Revcolevschi, Phys. Rev. B **54**, 15149 (1996).
[4] E. O. Wollan, W. C. Koehler, Phys. Rev. **100**, 545 (1955).
[5] G. S. Rushbrooke, G. S. Baker, Jr. and P. J. Wood in *Phase Transitions and Critical Phenomena* Vol. 3, Eds. C. Domb and M. S. Green, Academic Press (1974), Eqs. (1.1) and (5.4).
[6] A. J. Millis, Phys. Rev. B **55**, 6405 (1997).
[7] L. F. Feiner, A. M. Oleś, Physica B **259-261**, 796 (1999).
[8] H. Meskine, H. König, S. Satpathy, Phys. Rev. B **64** , 94433 (2001).
[9] D. D. Sarma, N. Shanthi, S. R. Barman, N. Hamada, H. Sawada, K. Terakura, Phys. Rev. Lett. **75**, 1126 (1995).
[10] W. E. Pickett, D. J. Singh, Phys. Rev. B **53**, 1146 (1996).
[11] I. V. Solovyev, N. Hamada, K. Terakura, Phys. Rev. Lett. **76**, 4825 (1996).
[12] I. V. Solovyev, N. Hamada, K. Terakura, Phys. Rev. B **53**, 7158 (1996).
[13] I. V. Solovyev, K. Terakura, Phys. Rev. Lett. **83**, 2825 (1999).
[14] M. Nicastro, M. Kuzmin, C. H. Patterson, Comp. Mater. Sci. **17**, 445 (2000).
[15] Y.-S. Su, T. A. Kaplan, S. D. Mahanti, J. F. Harrison, Phys. Rev. B **61**, 1324 (2000).
[16] G. S. Rushbrooke, G. S. Baker, Jr. and P. J. Wood in *Phase Transitions and Critical Phenomena* Vol. 3, Eds. C. Domb and M. S. Green, Academic Press (1974), Eq. (1.4).
[17] J. Rodriguez-Carvajal, M. Hennion, F. Moussa, A.H. Moudden, L. Pinsard, A. Revcolevschi, Phys. Rev. B **57**, R3189 (1998).
[18] J. B. A. A. Elemans, B. van Laar, K. R. van der Veen, B. O. Loopstra, J. Solid State Chem. **3**, 238 (1971).
[19] B. C. Tofield, W. R. Scott, J. Solid State Chem. **10**, 183 (1974).
[20] J. A. M. van Roosmalen *et al.* , J. Solid State Chem. **93**, 212 (1991); *ibid* **110** 100 (1994); *ibid* **110** 106 (1994).
[21] P. Norby *et al.* , J. Solid State Chem. **119**, 191 (1995).
[22] J. F. Mitchell *et al.* , Phys. Rev. B **54**, 6172 (1996).
[23] Q. Huang *et al.* , Phys. Rev. B **55**, 14987 (1997).
[24] J. B. Goodenough, Phys. Rev. **100**, 564 (1955).
[25] R. L. Martin, P. J. Hay, J. Chem. Phys. **98**, 8680 (1993).
[26] R. L. Martin, F. Illas, Phys. Rev. Lett. **79**, 1539 (1997).
[27] I. de P. R. Moreira, F. Illas, Phys. Rev. B **55**, 4129 (1997).
[28] GAMESS-UK is a package of *ab initio* programmess written by M. F.Guest, J. H. Lenthe, J. Kendrick, K. Schoffel, and P. Sherwood, with contributions from R. D. Amos, R. J. Buenker, H. J. J. van Dam, M. Dupuis, N. C. Handy, I. H. Hillier, P. J. Knowles, V. Bonacic-Koutecky, W. von Niessen, R. J. Harrison, A. P. Rendell, V. R. Saunders, A. J. Stone, D. J. Tozer, and A. H. de Vries. The package is derived from the original GAMESS code due to M. Dupuis, D. Spangler and J. Wendoloski, NRCC Software Catalog, Vol. 1, Program No. QG01 (GAMESS), 1980.
[29] Fermion eigenstates of a Hamiltonian which does not explicitly contain spin may be written

as anti-symmetric products of spatial orbitals and spin eigenfunctions (SEF's)[30]. SEF's are eigenfunctions of the total spin operator, $\hat{S}^2$, and $\hat{S}_z$ operator. SEF's may be generated in several different ways and the Multi-Reference Doubles CI module[31] of the GAMESS[28] code used in this work uses the Yamanouchi-Kotani (YK) scheme[32]. There is one SEF for six electrons coupled into a septet state while there are five SEF's for six electrons coupled into a singlet state. Each SEF consists of an orthonormal combination of products of the one-electron eigenspinors, α or β.

[30] R. Pauncz, *Spin Eigenfunctions: Construction and Use*, (Plenum Press, New York, 1979).

[31] R. J. Buenker, Studies in Physical and Theoretical Chemistry, **21**, 17 (1982).

[32] T. Yamanouchi, Proc. Phys. Math. Soc. Jpn. 18, 623 (1936); M. Kotani, A. Amemiya, E. Ishiguro and T. Kimura, *Tables of Molecular Integrals*, 2nd Ed. (Maruzen, Tokyo, 1963).

[33] A. Szabo, N. S. Ostlund, *Modern Quantum Chemistry: Introduction to Advanced Electronic Structure Theory*, (MacMillan, New York, 1982).

[34] V.R. Saunders, R. Dovesi, C. Roetti, M. Causá, N. M. Harrison, R. Orlando, C. M. Zicovich-Wilson, Crystal98 User's Manual, University of Torino, Torino, 1988. (www.cse.dl.ac.uk/Activity/CRYSTAL)

[35] Sums of SAF occupancies are slightly less than unity for states other than the fundamental SAF state because large numbers of SAF's with coefficients smaller than 0.003, which individually contribute 0.000009 to the total SAF occupancy, were omitted from the sums.

[36] The correlation energy for a molecule, cluster, *etc.* is usually defined to be the energy difference between that of an SCF wave function and a correlated wave function. Here the correlation energy is defined to be the difference between the fundamental SAF energy for each state and the energy when fluctuations within the limited active space described above are taken into account. Additional correlation energies, for example those due to fluctuations within an O ion, will be larger. However, it is believed that the correlation effects included in this work are the most important in determining exchange constants.

[37] C. M. Zicovich-Wilson, LoptCG Script, available from www.ch.unito.it/ifm/teorica/LoptCG.html

[38] R. D. Shannon and C. T. Prewitt, Acta Crystallogr. A **32** , 785 (1976).

[39] A. J. Millis, Phys. Rev. B **53**, 8434 (1996).

[40] These are plots of the difference in the charge density obtained from the UHF wave functions of the solid and superimposed (spherical) densities of Mn^{4+} ions with half-filled t_{2g} shells and O^{2-} ions. The plots therefore show the charge density of the Mn e_g electron and the distortion in density of an O^{2-} ion in the solid state.

[41] The 54 electron core LANL pseudopotential was used. P. J. Hay and W. R. Wadt, J. Chem. Phys. **82** , 270 (1989).

[42] T. Mizokawa, D. I. Khomskii, G. A. Sawatzky, Phys. Rev. B **60**, 7309 (1999).

[43] G. Zheng and C. H. Patterson (to be published).

[44] www.ch.unito.it/ifm/teorica/Basis-Sets/mendel.html

[45] M. D. Towler, Phys. Rev. B 50, 5041 (1994).

[46] W. C. Mackrodt Phil. Mag. A 68, 653 (1993).

[47] S. Foster, S. F. Boys, Rev. Mod. Phys. **32**, 296 (1960).

[48] The basis set is unpublished but is available at: www.tcm.phy.cam.ac.uk/ mdt26/crystal.html.

FIGURES

FIG. 1. *Pnma* structure of $LaMnO_3$ according to Elemans[18]. Mn-O bonds are shown explicitly. Mn ions are dark spheres, O ions are light spheres and La ions are unconnected light spheres. Mn ions labelled 1 and 2 are AF coupled ($J_\perp$) and Mn ions labelled 2 and 3 are FM coupled ($J_\parallel$). The cluster used to compute the AF coupling constant had the same structure as Mn ions 1 and 2 and their associated O^{2-} ion quasi-octahedra. The cluster used to compute the FM coupling constant had the same structure as Mn ions 2 and 3 and their associated O^{2-} ion quasi-octahedra.

FIG. 2. Empty orbital ordering in $LaMnO_3$. (A) The empty orbital arrangement which results when occupied orbitals are $d_{x^2-y^2}$ $d_{x^2-y^2}$ ordered. (B) Empty orbital arrangement with AF spin coupling favoured, (C) empty orbital arrangement with FM spin coupling favoured, (D) empty orbital arrangement with weak spin coupling.

FIG. 3. Localised orbital basis used for $CaMnO_3$ cluster CI calculations. Top panel: O $2p_z$ orbital; middle panel: Mn d_{xz} orbital; bottom panel:Mn $d_{3z^2-r^2}$ orbital. The latter is the empty e_g orbital responsible for exchange coupling.

FIG. 4. Localised orbital basis used for $J_\perp$ exchange constant cluster CI calculation for $LaMnO_3$. Top panel O $2p_z$ orbital; middle panel: filled e_g orbital perpendicular to Mn-O-Mn axis; bottom panel: empty e_g orbital oriented along Mn-O-Mn axis.

FIG. 5. Exchange coupling constants for $CaMnO_3$ and $LaMnO_3$ from CI cluster calculations with varying Mn ion Mulliken populations. The variation in Mulliken population was induced by changing the magnitude of point charges at Mn and La or Ca ion sites.

FIG. 6. Correlation energies in $CaMnO_3$ and $LaMnO_3$. Magnitudes of correlation energies are illustrated by vertical arrows and are given in meV in plain text. Energy differences between low and high multiplicity spin states are given in italics and occupancies of the fundamental SAF in each state are given at the base of each arrow. The horizontal line is the SCF ROHF energy for each state.

FIG. 7. Charge density difference plots for cubic $LaMnO_3$ with (a,b) $d_{3z^2-r^2}$ $d_{3z^2-r^2}$, (c,d) $d_{x^2-y^2}$ $d_{x^2-y^2}$, (e,f) $d_{x^2-y^2}$ $d_{3z^2-r^2}$ orbital ordering. Left and right panels show density differences in the xy and xz planes, respectively. The differences in charge densities are the UHF SCF density for the solid minus the UHF SCF densites for the O^{2-} ions and the Mn^{4+} ion.

FIG. 8. Total energies of $d_{x^2-y^2}$ $d_{x^2-y^2}$, $d_{3z^2-r^2}$ $d_{3z^2-r^2}$ and $d_{x^2-y^2}$ $d_{3z^2-r^2}$ orbital ordered structures with G-AF magnetic ordering. The reference energy is the cubic $LaMnO_3$ $d_{x^2-y^2}$ $d_{x^2-y^2}$ FM energy (Table V).

FIG. 9. Charge density difference plots for $LaMnO_3$ with a 5 percent Jahn-Teller distortion in the xy plane. Panels (a) and (b) show density differences in the xy and xz planes, respectively. The differences in charge densities are the UHF SCF density for the solid minus the UHF SCF densites for the O^{2-} ions and the Mn^{4+} ion.

TABLES

TABLE I. Relative energy and magnetic moment per Mn ion in $CaMnO_3$.

Spin Ordering	Relative Energy (meV)[a]	$\mu(\mu_B)$
FM	0.0	3.00
A-AF	-23.7	3.27
C-AF	-45.1	3.15
G-AF	-64.3	3.23

[a]Lattice constant 3.73 Å

TABLE II. Exchange constants in $CaMnO_3$ derived from experiment and *ab initio* calculations.

	J(meV)
Experiment[a]	6.6
Cluster CI[b]	8.1
Model Hamiltonian[c]	9.5
UHF[b]	10.7

[a]Rushbrooke *et al.*[5]
[b]This work. Lattice constant 3.73 Å
[c]Meskine *et al.*[8]

TABLE III. Relative energy and SAF occupation numbers for singlet and septet states of $Mn_2O_{11}^{14-}$ cluster representing $CaMnO_3$.

State	Energy (meV)[a]	Main SAF	t_{2g} Exchange	O to e_g (1e)	O to e_g (2e)
singlet[b]	+3.6	1.0000	0.0000	0.0000	0.0000
septet[b]	0	1.0000	0.0000	0.0000	0.0000
singlet[c]	-149.6	0.9926	0.0005	0.0038	0.0017
septet[c]	-133.4	0.9943	0.0000	0.0027	0.0017

[a]Energies are relative to the restricted open shell Hartree-Fock septet state
[b]Fundamental SAF only
[c]Fundamental SAF + all single and double excitations in active space from fundamental SAF

TABLE IV. Structural parameters in Jahn-Teller distorted $LaMnO_3$ and *Pnma* $LaMnO_3$ determined by experiment and total energy minimisation. Each cell is a $\sqrt{2}$x2x$\sqrt{2}$ doubling of the primitive perovskite unit cell.

Ion	x	y	z
La[a]	0.549	0.250	0.010
Mn	0.000	0.000	0.000
O	-0.014	0.250	-0.070
O	0.309	0.039	0.224
La[b]	0.517	0.250	0.001
Mn	0.000	0.000	0.000
O	-0.002	0.250	-0.027
O	0.290	0.014	0.237
La[c]	0.500	0.250	0.000
Mn	0.000	0.000	0.000
O	0.000	0.250	0.000
O	0.2625	0.000	0.2625

[a]Experimental structure[18] (Fig. 1), lattice parameters a=5.742Å, b=7.668Å, c=5.532Å
[b]Optimised structure, lattice parameters a=5.740Å, b=7.754Å, c=5.620Å
[c]Jahn-Teller distorted structure, lattice parameters a=5.590Å, b=7.905Å, c=5.590Å. Note that the Jahn-Teller distortion is in the xz plane in this Table to allow easy comparison between its structural parameters and those of the *Pnma* structures. Elsewhere in this work the Jahn-Teller distortion is assumed to be in the xy plane.

TABLE V. Relative energy and magnetic moment per Mn ion in cubic $LaMnO_3$ with various spin and orbital orderings.

Spin and Orbital Ordering[a]	Relative Energy (meV)	$\mu(\mu_B)$
FM $d_{x^2-y^2}$ $d_{x^2-y^2}$	0.0	4.00
FM $d_{x^2-y^2}$ $d_{3z^2-r^2}$	-131.5	4.00
FM $d_{3z^2-r^2}$ $d_{3z^2-r^2}$	-6.1	3.99
A-AF $d_{x^2-y^2}$ $d_{x^2-y^2}$	-14.4	4.05
A-AF $d_{3z^2-r^2}$ $d_{3z^2-r^2}$	-34.4	3.87
G-AF $d_{x^2-y^2}$ $d_{x^2-y^2}$	-34.9	3.88
G-AF $d_{x^2-y^2}$ $d_{3z^2-r^2}$	-95.4	3.89
G-AF $d_{3z^2-r^2}$ $d_{3z^2-r^2}$	-34.0	3.88

[a]Lattice constant 3.934Å

TABLE VI. Exchange constants in cubic $LaMnO_3$ with various orbital orderings.

Spin and Orbital Ordering[a]	$J_\perp$ (meV)[b]	$J_\parallel$ (meV)[c]
$d_{x^2-y^2}$ $d_{x^2-y^2}$	7.2	5.1
$d_{x^2-y^2}$ $d_{3z^2-r^2}$	-6.0	-6.0
$d_{3z^2-r^2}$ $d_{3z^2-r^2}$	14.2	-0.1

[a]Lattice constant 3.953Å
[b]Exchange constant for Mn ions coupled perpendicular to *ac* plane
[c]Exchange constant for Mn ions coupled parallel to *ac* plane

TABLE VII. Relative energy and magnetic moment per Mn ion in *Pnma* and Jahn-Teller distorted cubic $LaMnO_3$.

Structure and Spin Ordering	Energy(meV)	$\mu(\mu_B)$
Pnma (Experiment) FM[a]	0.0	4.00
Pnma (Experiment) A-AF	-1.2	4.00
Pnma (Experiment) G-AF	13.9	3.96
Pnma (Optimised) FM[b]	0.0	4.00
Pnma (Optimised) A-AF	-2.0	3.96
Pnma (Optimised) G-AF	21.9	3.94
Jahn-Teller FM[c]	0.0	4.00
Jahn-Teller A-AF	1.1	3.98
Jahn-Teller G-AF	33.6	-

[a]Reference energy is 194 meV above optimised FM *Pnma* structure (Table IV).
[b]Reference energy is that of this structure and magnetic order (Table IV).
[c]Reference energy is 8 meV below optimised FM *Pnma* structure (Table IV).

TABLE VIII. Exchange constants in *Pnma* $LaMnO_3$ derived from experiment and *ab initio* and model Hamiltonian calculations.

	$J_\perp$ (meV)[a]	$J_\parallel$ (meV)[b]
Experiment[c]	4.8	-6.7
UHF(Experiment)[d]	0.6	-3.7
UHF(Experiment)[e]	0.8	-3.5
UHF(Optimised)[f]	1.0	-6.0
UHF(Jahn-Teller)[g]	-0.6	-8.1
LSDA(Experiment)[h]	-3.1	-9.1
Cluster CI(Experiment)[d]	3.3	-3.6
Cluster CI(Optimised)[f]	5.1	-7.4
Cluster CI(Optimised/La pseudopotential)[f]	5.2	-7.4
model Hamiltonian[i]	4.8	-3.7

[a]Exchange constant for Mn ions coupled perpendicular to *ac* plane
[b]Exchange constant for Mn ions coupled parallel to *ac* plane
[c]Hirota *et al.*[2];Moussa *et al.*[3]
[d]This work. Elemans structure[18](Table IV).
[e]Su *et al.*[15].
[f]This work. Optimised structure (Table IV).
[g]This work. Jahn-Teller distorted structure (Table IV).
[h]Soloyev *et al.*[11].
[i]Meskine *et al.*[8]

TABLE IX. Relative energy and orbital occupation numbers for singlet and nonet states of $Mn_2O_{11}^{16-}$ cluster representing $LaMnO_3$.

State	Energy (meV)[a]	Main SAF	t_{2g} Exchange	O to e_g (1e)	O to e_g (2e)
singlet[bd]	+11.9	1.0000	0.0000	0.0000	0.0000
nonet[bd]	0.0	1.0000	0.0000	0.0000	0.0000
singlet[cd]	-93.5	0.9937	0.0006	0.0037	0.0007
nonet[cd]	-83.3	0.9954	0.0000	0.0030	0.0007
singlet[be]	+17.9	1.0000	0.0000	0.0000	0.0000
nonet[be]	0.0	1.0000	0.0000	0.0000	0.0000
singlet[ce]	-64.9	0.9949	0.0004	0.0025	0.0006
nonet[ce]	-79.9	0.9946	0.0000	0.0038	0.0008

[a]Energies are relative to the restricted open shell Hartree-Fock septet for the whole cluster, *i.e.* per Mn ion pair.
[b]Fundamental SAF only
[c]Fundamental SAF + all single and double excitations in active space from fundamental SAF
[d]$J_\perp$ calculation
[e]$J_\parallel$ calculation

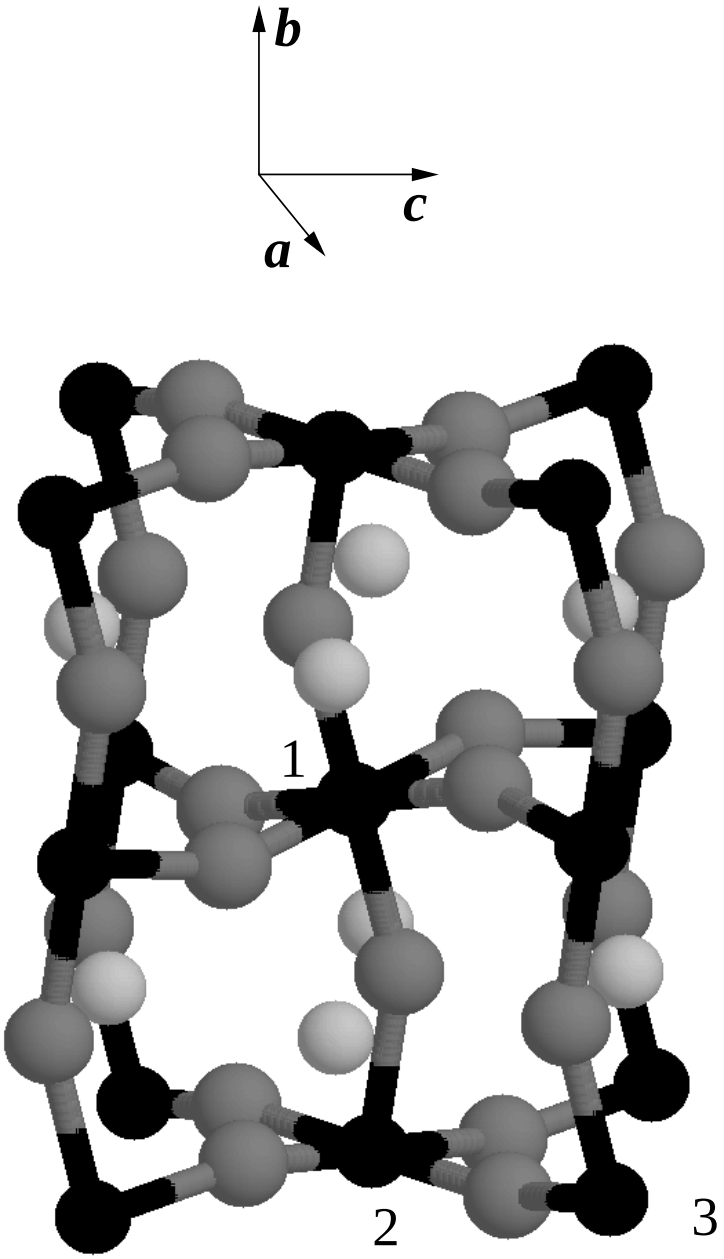
b
c
a
1
2
3

A

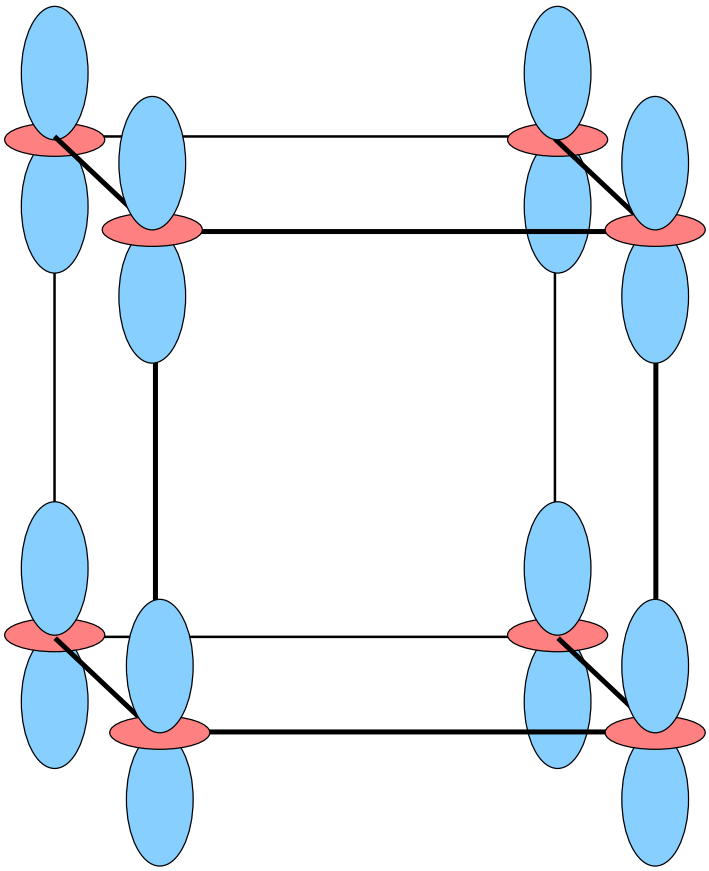

B

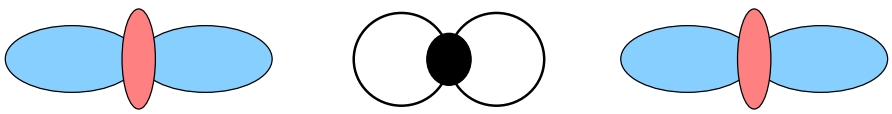

C

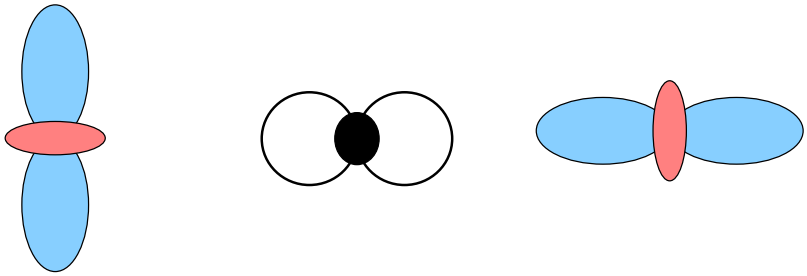

D

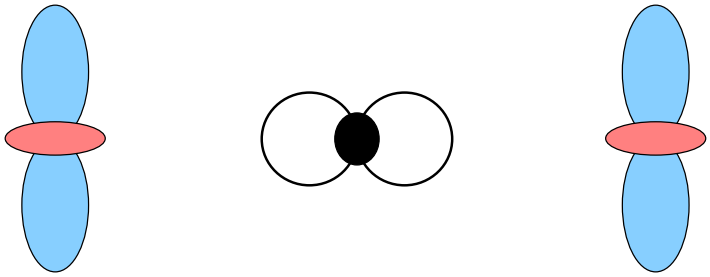

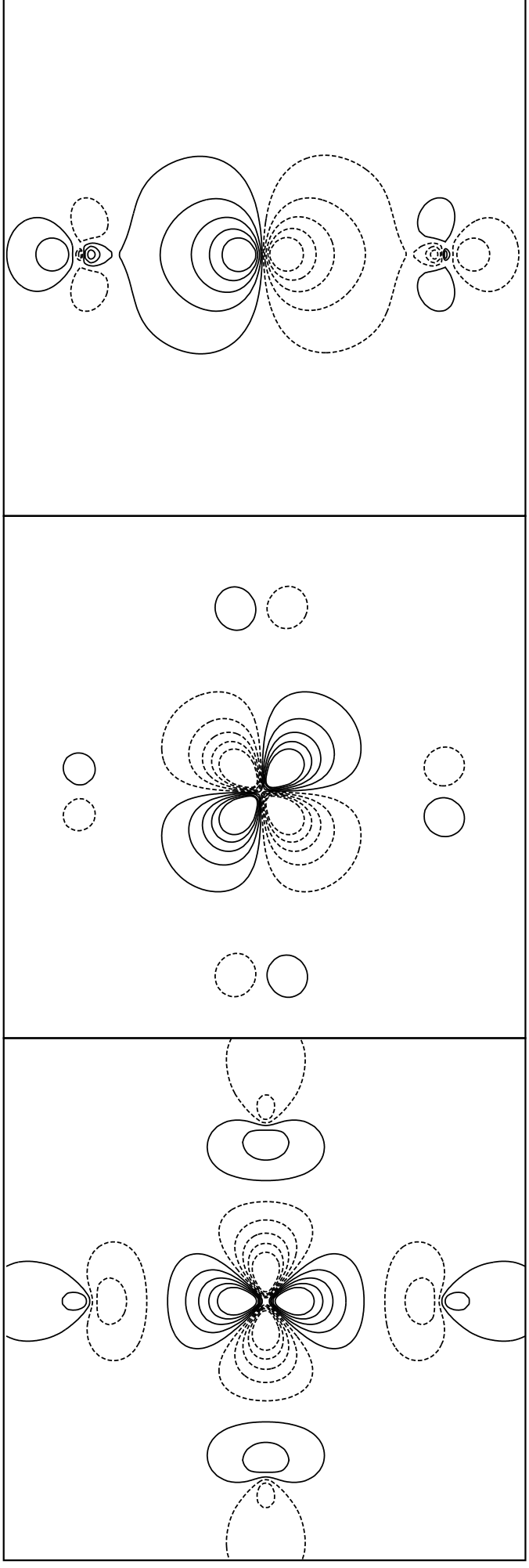

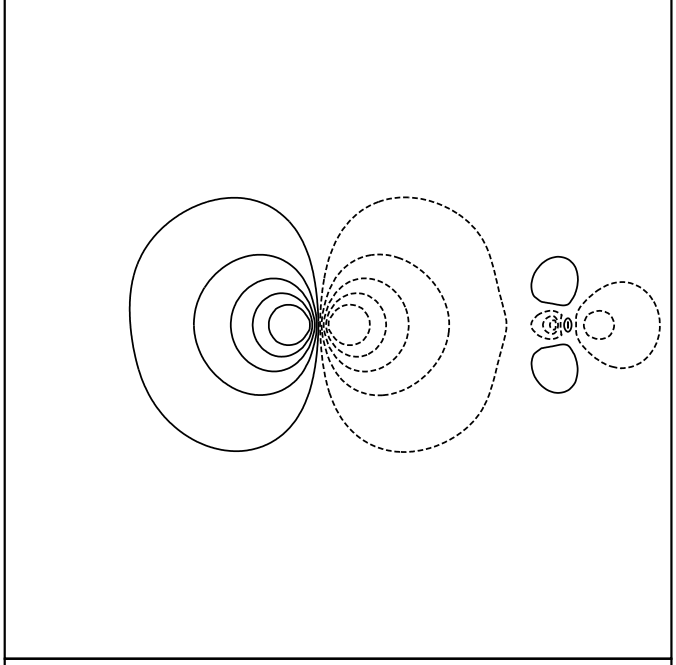

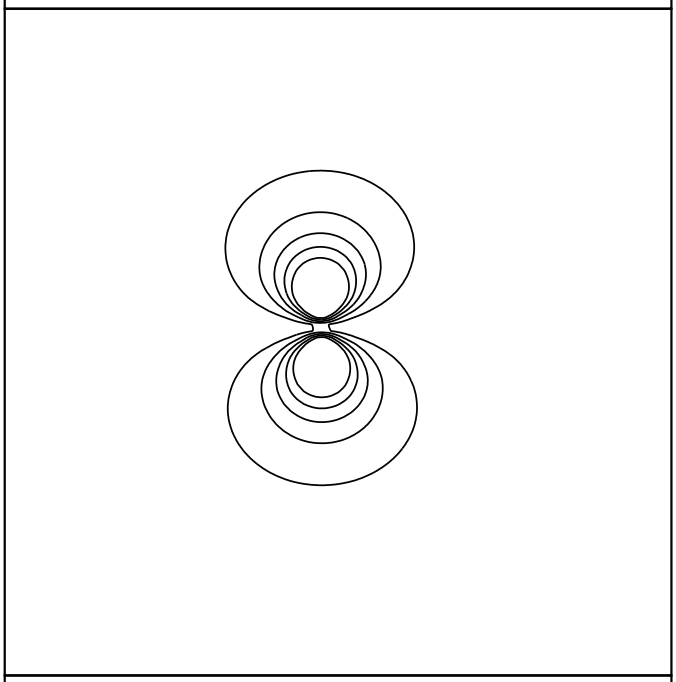

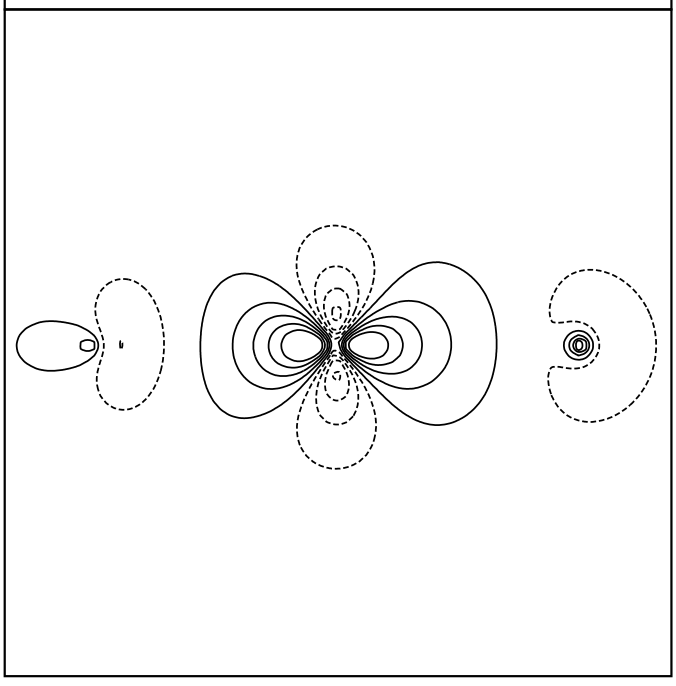

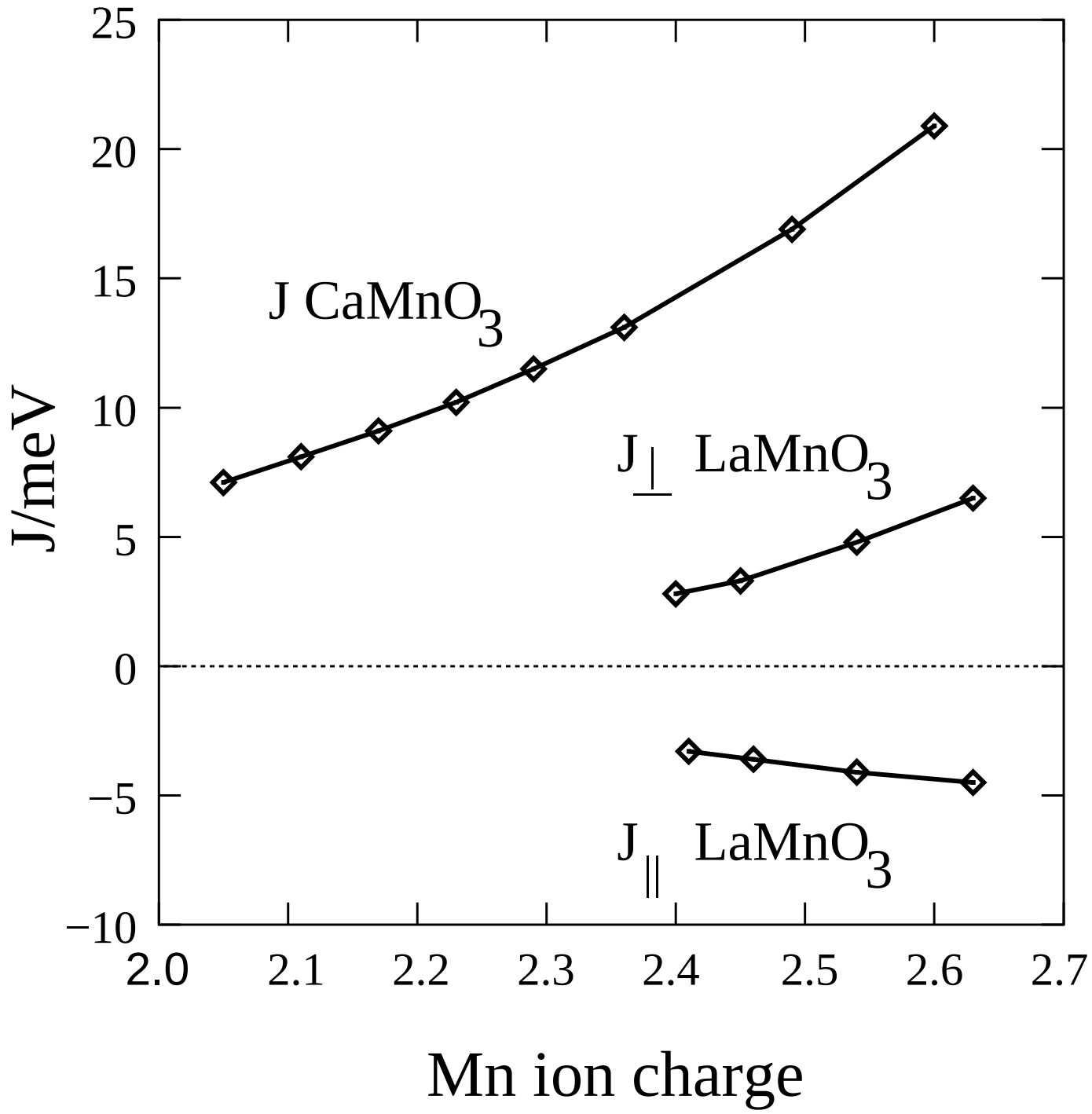
25
20
15
10
5
0
−5
−10
J/meV
J CaMnO3
J⊥ LaMnO3
J|| LaMnO3
2.0
2.1
2.2
2.3
2.4
2.5
2.6
2.7
Mn ion charge

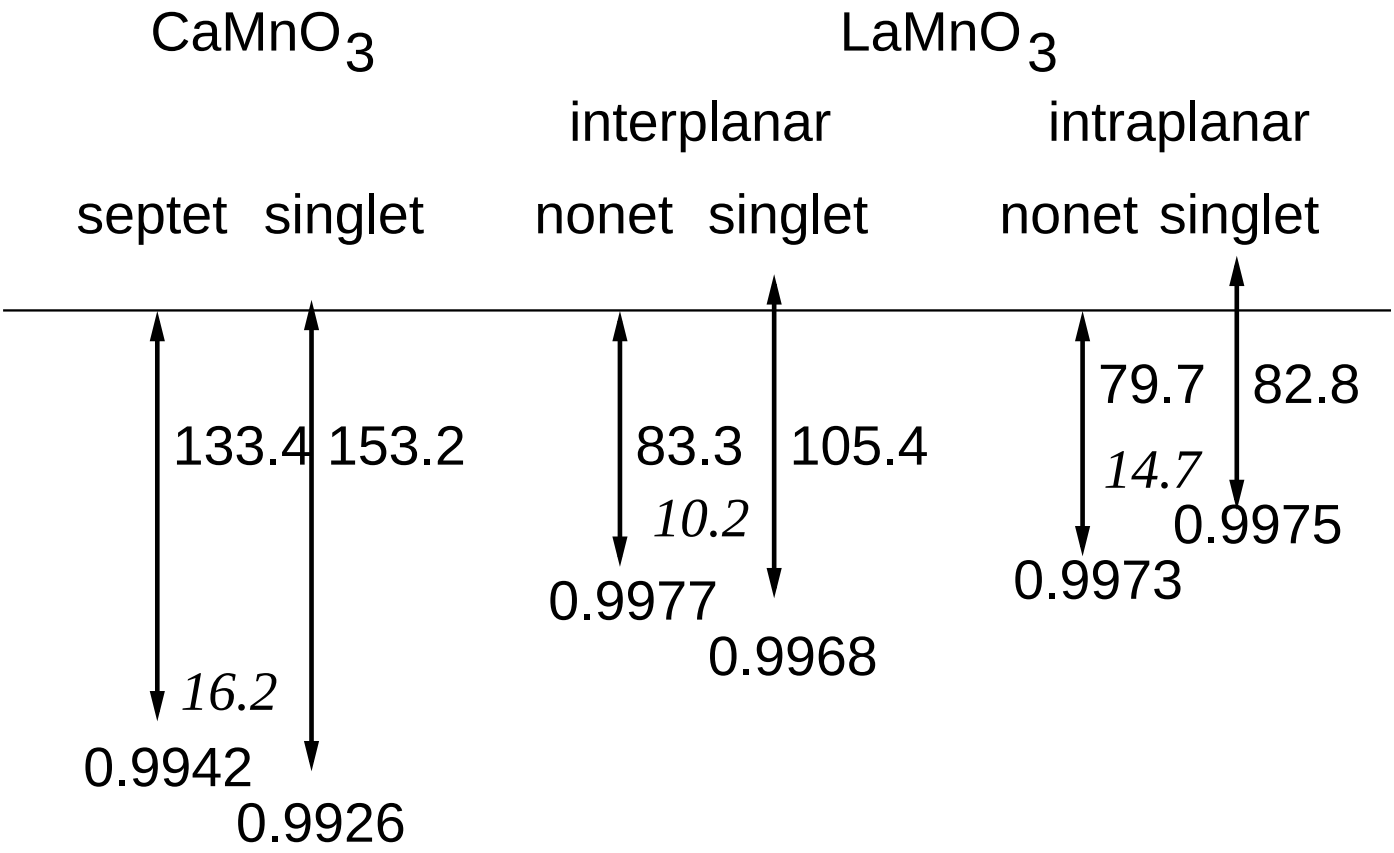
CaMnO3
LaMnO3
interplanar
intraplanar
septet
singlet
nonet
singlet
nonet
singlet
133.4
153.2
83.3
105.4
79.7
82.8
16.2
10.2
14.7
0.9942
0.9926
0.9977
0.9968
0.9973
0.9975

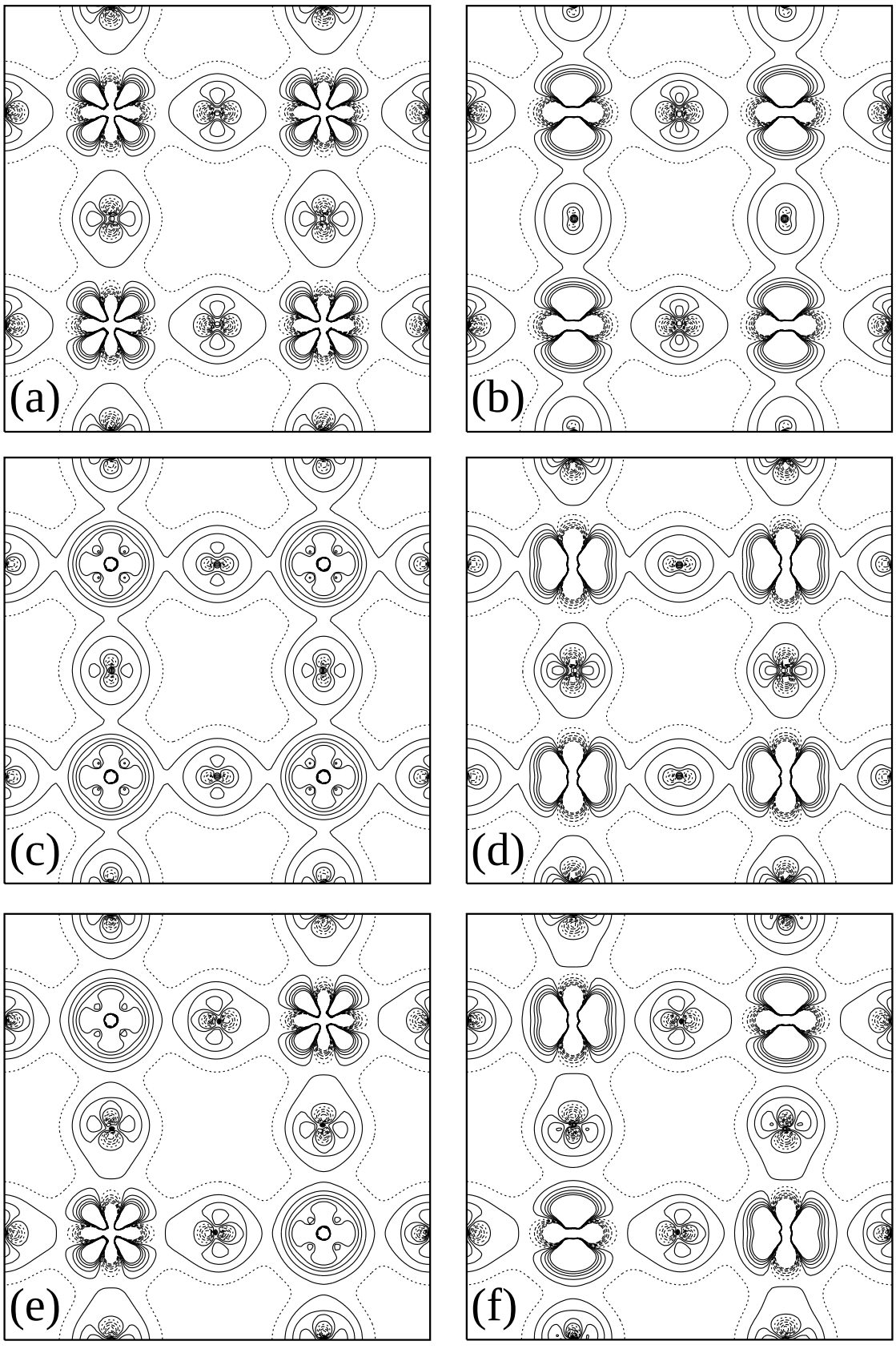
(a)
(b)
(c)
(d)
(e)
(f)

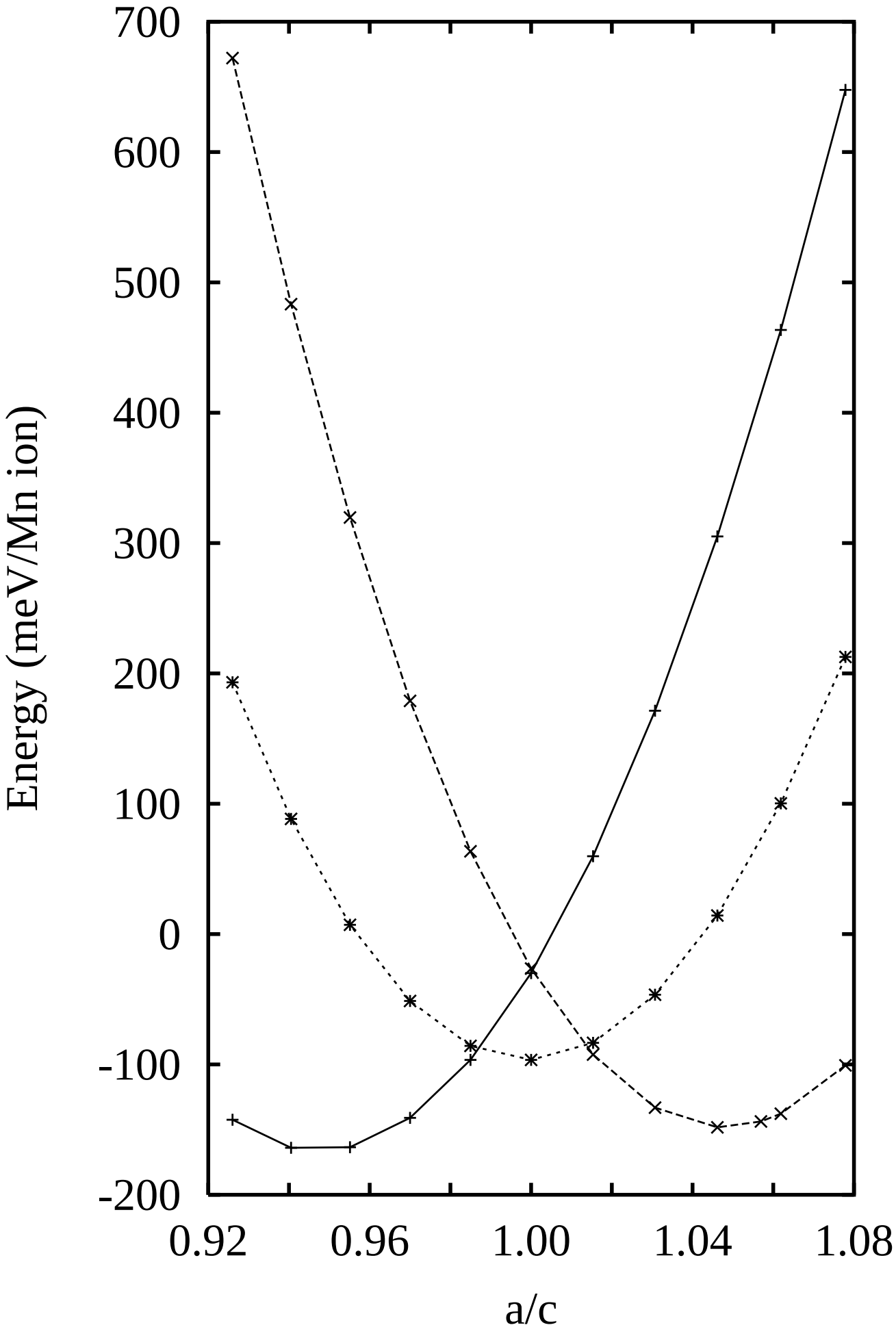
700
600
500
400
300
200
100
0
-100
-200
Energy (meV/Mn ion)
0.92
0.96
1.00
1.04
1.08
a/c

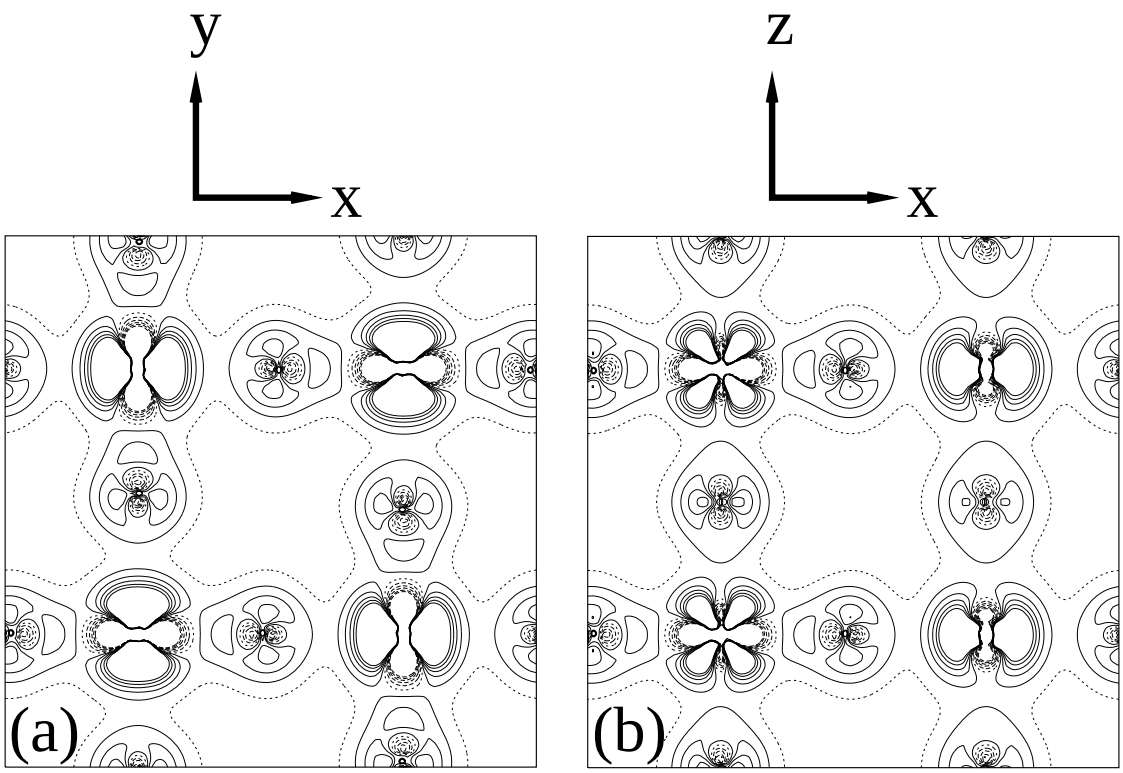
y
x
z
x
(a)
(b)